THE UNIVERSITY of EDINBURGH

Edinburgh Research Explorer

The immobilisation and reactivity of Fe(CN)6 3/4 in an intrinsically microporous polyamine (PIM-EA-TB)

OPEN ACCESS

ORIGINAL PAPER

The immobilisation and reactivity of $Fe(CN)_6^{3-/4-}$ in an intrinsically microporous polyamine (PIM-EA-TB)

Lina Wang[1] · Richard Malpass-Evans[2] · Mariolino Carta[3] · Neil B. McKeown[2] · Frank Marken[1]

Abstract

Protonation of the molecularly rigid polymer of intrinsic microporosity PIM-EA-TB can be coupled to immobilisation of $Fe(CN)_6^{3-/4-}$ (as well as immobilisation of Prussian blue) into 1–2 nm diameter channels. The resulting films provide redox-active coatings on glassy carbon electrodes. Uptake, transport, and retention of $Fe(CN)_6^{3-/4-}$ in the microporous polymer are strongly pH dependent requiring protonation of the PIM-EA-TB ($pK_A \approx 4$). Both $Fe(CN)_6^{4-}$ and $Fe(CN)_6^{3-}$ can be immobilised, but $Fe(CN)_6^{4-}$ appears to bind tighter to the polymer backbone presumably via bridging protons. Loss of $Fe(CN)_6^{3-/4-}$ by leaching into the aqueous solution phase becomes significant only at pH > 9 and is likely to be associated with hydroxide anions directly entering the microporous structure to combine with protons. This and the interaction of $Fe(CN)_6^{3-/4-}$ and protons within the molecularly rigid PIM-EA-TB host are suggested to be responsible for retention and relatively slow leaching processes. Electrocatalysis with immobilised $Fe(CN)_6^{3-/4-}$ is demonstrated for the oxidation of ascorbic acid.

Introduction

Ferrocyanide, $Fe(CN)_6^{4-}$, is a well-studied redox mediator and homogeneous one-electron electrocatalyst (see Eq. 1). Ferrocyanide has previously been employed as a redox mediator in electro-organic transformations [1], as an electron shuttle for respiring living cells [2], in thermoelectrochemical devices [3], in the electroanalytical determination of ascorbate [4], nitrite [5], hydrogen sulphide [6, 7] or (via electrochemiluminescence) in the determination of thiols [8]. Ferrocyanide has been employed also as heterogeneous or polymer-immobilised redox catalyst for sulphide detection [9] and for nitrite detection [10]. Ferrocyanide is known to form a diverse range of inorganic coordination polymers

[11]. Particularly, the water insoluble Prussian blue analogues [12] and related coordination polymers [13] have been widely investigated, for example for applications in sensing [14, 15] and in biosensing [16, 17]. The solid-state electrochemical properties of Prussian blue analogues have been investigated systematically by Scholz and co-workers [18–20]. Only very recently has a new type of complex formation of $Fe(CN)_6^{4-}$ with organic ammonium cations been exploited to also give a range of "organic–Prussian blues" [21]. Here, an amine-containing polymer of intrinsic microporosity (PIM) with molecularly rigid nanochannels is investigated as a host for the $Fe(CN)_6^{3-/4-}$ redox mediator. Note that the abbreviation "PIM" has also been employed for the unrelated photo-induced magnetism effect in Prussian blue analogues [22–24]:

$$Fe(CN)_6^{3-} + e^- \quad Fe(CN)_6^{4-} \tag{1}$$

Polymers of intrinsic microporosity (PIMs [25]) have been developed as a new class of molecularly rigid backbone materials with properties such as (i) high microporosity and surface area [26–28], (ii) controlled gas permeation and separation [29], (iii) good solubility and processability [30], and (iv) potential for applications in electrochemical systems [31] and membranes [32]. Here, the microporous material PIM-EA-TB is employed ("EA" = ethanoanthracene and "TB" = Tröger base [33], see molecular structure in Fig. 1). The effects of

✉ Frank Marken
   f.marken@bath.ac.uk

[1] Department of Chemistry, University of Bath, Claverton Down, Bath BA2 7AY, UK

[2] EaStCHEM, School of Chemistry, University of Edinburgh, Joseph Black Building, David Brewster Road, Edinburgh, Scotland EH9 3JF, UK

[3] Department of Chemistry, Swansea University, College of Science, Grove Building, Singleton Park, Swansea SA2 8PP, UK

"fractional free volume" in rigid microporous polymer structures on ion transport and conductivity have been considered [34]. In PIM-EA-TB, there are "free volume elements" providing multiple amine site, which after protonation allow anion binding into "cavities". Experimentally, it was observed that more hydrophobic alcohols can partition into redox catalyst–modified PIM-EA-TB [35], and that hydrophobic anions such as perchlorate interact with/permeate through PIM-EA-TB [36]. Here, the case of multiple-charged anions such as $Fe(CN)_6^{3-/4-}$ is investigated. Interactions based on hydrophobicity of the polymer host environment can be complemented by ionic interaction and by hydrogen bonding, as demonstrated in this study.

Organic–Prussian blues can be divided into (i) organic materials that bind $Fe(CN)_6^{3-/4-}$ anions (e.g. polymers containing imidazolium [37]) and (ii) hybrid materials based on organic components and Prussian blue-type components. There are many types of hybrid architectures, for example layer-by-layer structures for hybrid polymer–Prussian blue films [38] with application in sensor film [39]. Organic–Prussian blue hybrid materials have been employed in electrochromic devices [40] and films [41, 42]. Polymer–Prussian blue hybrid materials have been obtained as 2D nanoarchitectures [13], and tetra-alkylammonium cations have been incorporated into Prussian blue analogues [43].

Non-organic hollow Prussian blue analogue structures have been obtained for applications in energy storage [44], and Prussian blues embedded into other types of coordination metal-organic structures have been reported [45]. The immobilization of ferrocyanide into polyamine structures has been reported [5]. The protonation of ferrocyanide has been shown to lead to aggregation (via hydrogen bridges) and to network structures with a range of organic amines [21].

Here, PIM-EA-TB is investigated as a microporous coating on electrode surfaces. The tertiary amines in the polymer backbone are shown to undergo protonation to then "trap" $Fe(CN)_6^{4-}$ and/or $Fe(CN)_6^{3-}$ anions. The pK_A for the protonation of PIM-EA-TB has been previously estimated as $pK_A \approx$

Fig. 1 Schematic drawing to illustrate the molecular structure of PIM-EA-TB and protonation coupled to anion binding with an apparent pK_A that is shifted into the alkaline region in the presence of $Fe(CN)_6^{4-}$

4 for hydrophilic anions [46]. Here, protonation of PIM-EA-TB is shown to be associated with the binding of sterically demanding $Fe(CN)_6^{4-}$ or $Fe(CN)_6^{3-}$ anions (with ionic diameters of 450 pm and 440 pm, respectively [47]) from aqueous solution. These highly charged anions are likely to carry cations such as H^+ or K^+ to further increase their size during transport through rigid pores of diameter 1–2 nm in PIM-EA-TB [48]. It is shown that the presence of the $Fe(CN)_6^{3-/4-}$ anions in PIM-EA-TB leads to an apparent shift in the polymer pK_A by approximately 5 units, thereby providing a novel film electrode with embedded $Fe(CN)_6^{3-/4-}$ and with catalytic properties. In part, this behaviour is linked to the first protonation equilibrium for $Fe(CN)_6^{3-/4-}$ with $pK_{A,Fe(CN)64-} = 4.2$ and $pK_{A,Fe(CN)63-} < 1$ at 25 °C [49, 50].

Experimental

Chemical reagents

Potassium ferrocyanide (98.5–102.0%), potassium ferricyanide (> 99.0%), potassium chloride (99.0–100.5%), hydrochloric acid (37%), chloroform (≥ 99.8%), potassium hydroxide (≥ 85%) and L-ascorbic acid (≥ 99%) were purchased from Sigma Aldrich and were used as received without further purification. PIM-EA-TB was synthesised according to the literature recipe [33]. Aqueous solutions were prepared with ultrapure water of resistivity not less than 18.2 MΩ cm (at 20 °C) from a Thermo Scientific water purification system.

Instrumentation

Electrochemical experiments were performed with a potentiostat (Metrohm μAutolab II) with a conventional three-electrode system, where a Pt wire was the counter electrode, a 3-mm diameter glassy carbon disk electrode was employed as a working electrode, and a KCl-saturated calomel electrode (SCE, Radiometer REF401) acted as the reference. In experiments exploring pH effects, the pH of the 0.1 M KCl solutions was adjusted by adding 1 M HCl or 1 M KOH and monitored with a pH meter (Jenway 3505). The cross-section morphology of the PIM-EA-TB film deposits was imaged by using a field emission scanning electron microscope (JEOL JSM-6301F FESEM).

Procedures

A solution of 1 mg/mL PIM-EA-TB was prepared by dissolving the polymer in chloroform. Typically, 2 μL of PIM-EA-TB solution was deposited onto a 3-mm diameter glassy carbon electrode to form a film deposit. After drying under ambient conditions, a uniform coating is obtained with estimated 1–2 μm thickness (see Fig. 2). Then, the electrode was
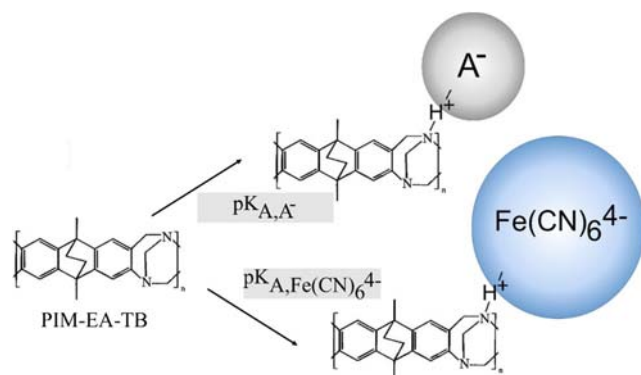
immersed into $Fe(CN)_6^{4-}$ or $Fe(CN)_6^{3-}$ dissolved in aqueous HCl solution to carry out protonation and immobilisation for typically 12 h at 4 °C in the dark (in a refrigerator). The SEM images for films before and after $Fe(CN)_6^{4-}$ immobilisation were essentially identical.

Results and discussion

Concentration effects on binding and reactivity of $Fe(CN)_6^{3-/4-}$ in PIM-EA-TB

Initial experiments were performed by coating PIM-EA-TB (typically 2 μL of 1 mg/mL solution in chloroform to give a 2-μg deposit on 7×10^{-6} m^2 corresponding to roughly 0.3 μm average thickness with 1 g cm^{-3} assumed density; given a monomer molecular weight of 300 g mol^{-1}, this corresponds to 6 nmol of monomeric unit) onto a glassy carbon disk electrode (diameter 3 mm) and immersion of this electrode into $Fe(CN)_6^{4-}$ dissolved in aqueous 1 mM HCl (pH approx. 3). The hydrochloric acid ensures protonation of the PIM-EA-TB and thereby drives the binding of the $Fe(CN)_6^{4-}$ anion over 12 h at 4 °C in the dark. Experiments with the same solution in the presence of light and at room temperature result in the formation of PIM-embedded Prussian blue instead. Figure 3 shows photographs of the blue-green (Prussian blue precursor containing) solution of 1 mM $Fe(CN)_6^{4-}$ in 1 mM HCl after 24 h under ambient conditions in the light (A) and the pristine solution after 24 h at 4 °C in the dark (B). Voltammetric data for both types of electrodes obtained after rinsing with water and transfer into aqueous 0.1 M KCl with 1 mM HCl are shown in Fig. 3 c and d. Well-defined highly reversible voltammetric peaks are obtained after immobilisation at 4 °C. Experimental current data obtained under these conditions for freshly prepared electrodes are reproducible within ± 10%, but there are many subtle factors affecting the outcome of experiments as will be shown below. For electrodes prepared at room temperature, lower peak currents are observed and a considerable peak shape distortion results probably from the presence of Prussian blue fragments or $Fe(CN)_6^{4-}$

decomposition products formed under acidic conditions [51] within the micropores of the PIM-EA-TB host.

These cyclic voltammetry responses are for thin films immobilised on the electrode surface and therefore not directly comparable to data obtained for the bare glassy carbon electrode immersed in aqueous 0.1 M KCl with 2 mM $Fe(CN)_6^{4-}$ and 2 mM $Fe(CN)_6^{3-}$, but it is interesting to compare the midpoint potentials. Data in Fig. 3d for a scan rate of 10 mV s^{-1} suggest an oxidation peak at 0.214 V vs. SCE and a reduction peak at 0.135 V vs. SCE. This in turn suggests a midpoint potential of $E_{mid} = ½ (E_{p,ox} + E_{p,red}) = 0.175$ V vs. SCE. In the absence of the polymer film, the corresponding value is $E_{mid} = 0.193$ V vs. SCE. The slight negative shift in potential in the presence of the polymer is relatively minor. It may indicate a slightly stronger binding to $Fe(CN)_6^{3-}$ relative to that for $Fe(CN)_6^{4-}$, but other factors such as polymer | electrolyte interfacial potentials may also play a role.

In the following experiments, immobilisation of $Fe(CN)_6^{4-}$ or of $Fe(CN)_6^{3-}$ is performed always at 4 °C in the dark. The electrode is then rinsed and transferred into an electrochemical cell with aqueous 0.1 M KCl containing 1 mM HCl. Figure 4 a shows cyclic voltammograms (scan rate 0.1 Vs^{-1}) for immobilisation experiments employing (i) 0.01, (ii) 0.1, and (iii) 1 mM $Fe(CN)_6^{4-}$. In all cases, binding of $Fe(CN)_6^{4-}$ occurs and stable (time-independent over at least 10 potential cycles) cyclic voltammetry responses are obtained.

When testing the effect of $Fe(CN)_6^{4-}$ concentration during the immobilisation process, a clear increase in voltammetric peak current is observed when going from 0.01 mM to 0.1 mM $Fe(CN)_6^{4-}$. Perhaps surprisingly, for a higher concentration of 1 mM $Fe(CN)_6^{4-}$, the voltammetric peak current decreases again. That is, increasing the content of $Fe(CN)_6^{4-}$ in the immobilisation solution appears to be detrimental to the immobilisation process. Even more dramatic is the effect of immobilisation in 10 mM $Fe(CN)_6^{4-}$ (not shown), where the resulting voltammetric current peaks are very low, similar to those observed for 0.01 mM $Fe(CN)_6^{4-}$. Leaving the immobilisation process to continue for 5 days causes complete loss of signal. This behaviour is consistent with $Fe(CN)_6^{4-}$ acting as a base with $pK_A \approx 4.2$ [49, 50]. The presence of this base then causes a lower degree of polymer protonation and
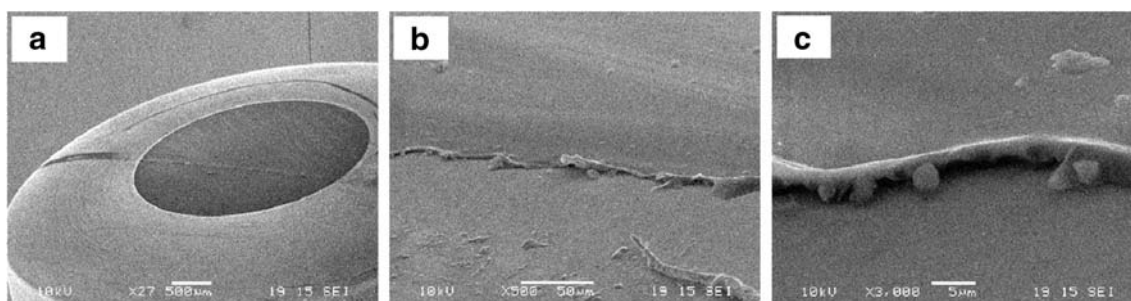

Fig. 2 Scanning electron microscopy images for **a** a 3-mm diameter glassy carbon electrode partially covered with PIM-E-TB, **b** a closer look at the polymer film edge and **c** a higher magnification image of the PIM-EA-TB film edge

Fig. 3 **a** Photograph of 1 mM Fe(CN)$_6^{4-}$ in 1 mM HCl left in 24 h ambient light and room temperature. **b** The same solution left 24 h at 4 °C in a refrigerator. **c** Cyclic voltammograms (first cycle; scan rate (i) 10, (ii) 20, (iii) 50, (iv) 100, (v) 200, (vi) 500 mVs^{-1}) for a 3-mm diameter glassy carbon electrode coated with 2 μg PIM-EA-TB after 12 h immersion in 1 mM Fe(CN)$_6^{4-}$ in 1 mM HCl at room temperature. **d** As above but for a sample kept at 4 °C for 12 h in the dark
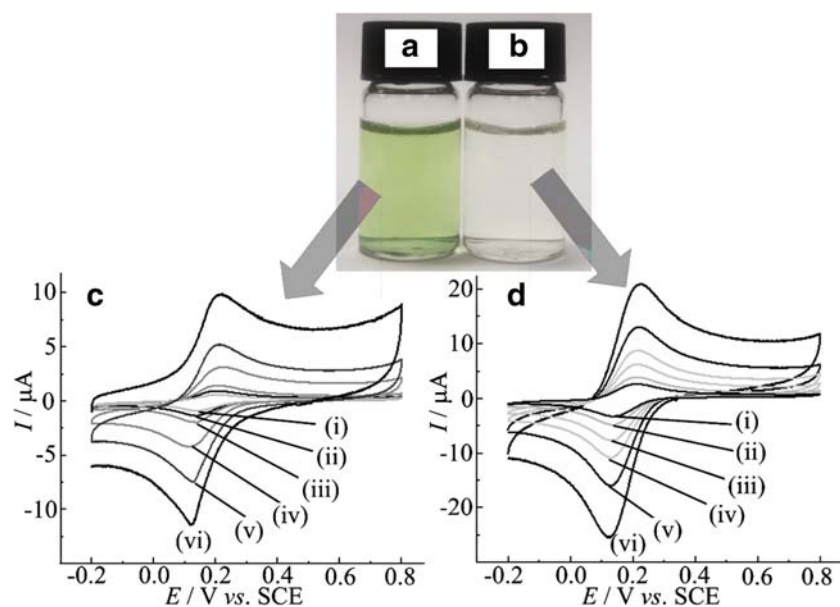
therefore less Fe(CN)$_6^{4-}$ is immobilised. The absence of a voltammetric response when attempting immobilisation of Fe(CN)$_6^{4-}$ without protons into PIM-EA-TB is consistent with the recently reported low permeation of Fe(CN)$_6^{4-}$ under conditions of redox flow battery application [52].

When performing similar experiments with Fe(CN)$_6^{3-}$, again, immobilisation of the redox-active anion into PIM-EA-TB is observed. Figure 4 b shows a similar trend in voltammetric current responses again with a maximum peak current for 0.1 mM Fe(CN)$_6^{3-}$ concentration. Due to the lower pK$_A$ for Fe(CN)$_6^{3-}$, direct competition for protons may be less

likely, but a similar reason for the observed concentration dependence of immobilisation process has to be assumed. Voltammetric currents in this case appear to be slightly lower in general with a more symmetric peak (a lower peak-to-peak separation) possibly indicating more limited thin film charge transport.

The effect of scan rate on the voltammetric currents is investigated next for immobilisation of 0.1 mM Fe(CN)$_6^{4-}$ (Fig. 5a) and for immobilisation of 0.1 mM Fe(CN)$_6^{3-}$ (Fig. 5b). In both cases, voltammetric responses are investigated in 0.1 M KCl containing 1 mM HCl. When immobilising

Fig. 4 **a** Cyclic voltammograms (first cycle; scan rate 0.1 Vs^{-1}) for a 3-mm diameter glassy carbon electrode coated with 2 μg PIM-EA-TB after 12 h immersion in (i) 0.01, (ii) 0.1, and (iii) 1 mM Fe(CN)$_6^{4-}$ in 1 mM HCl. **b** As before, but for immobilisation in (i) 0.01, (ii) 0.1, and (iii) 1 mM Fe(CN)$_6^{3-}$ in (i) 0.01, (ii) 0.1, and (iii) 1 mM HCl. **c** Schematic drawing of the proposed electron pathway during electron hopping
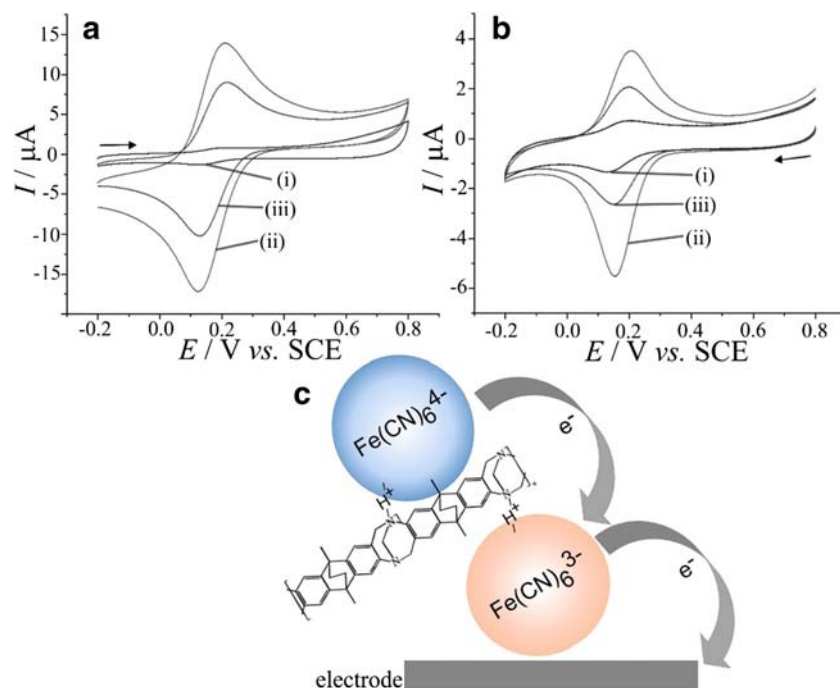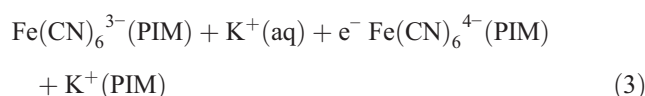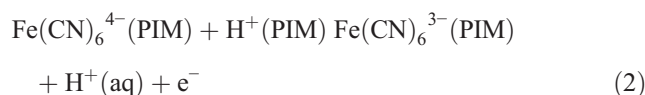
Fig. 5 **a** Cyclic voltammograms (first cycle; scan rate (i) 10,(ii) 20, (iii) 50, (iv) 100, (v) 200, (vi) 500 mVs^{-1}) for a 3-mm diameter glassy carbon electrode coated with 2 μg PIM-EA-TB (after 12 h immersion in 0.1 mM Fe(CN)$_6^{4-}$ in 1 mM HCl at 4 °C) immersed in 0.1 KCl/1 mM HCl. **b** Double-logarithmic plot of anodic peak current versus scan rate. **c** As above, but for Fe(CN)$_6^{3-}$. **b** Double-logarithmic plot of ca-thodic peak current versus scan rate
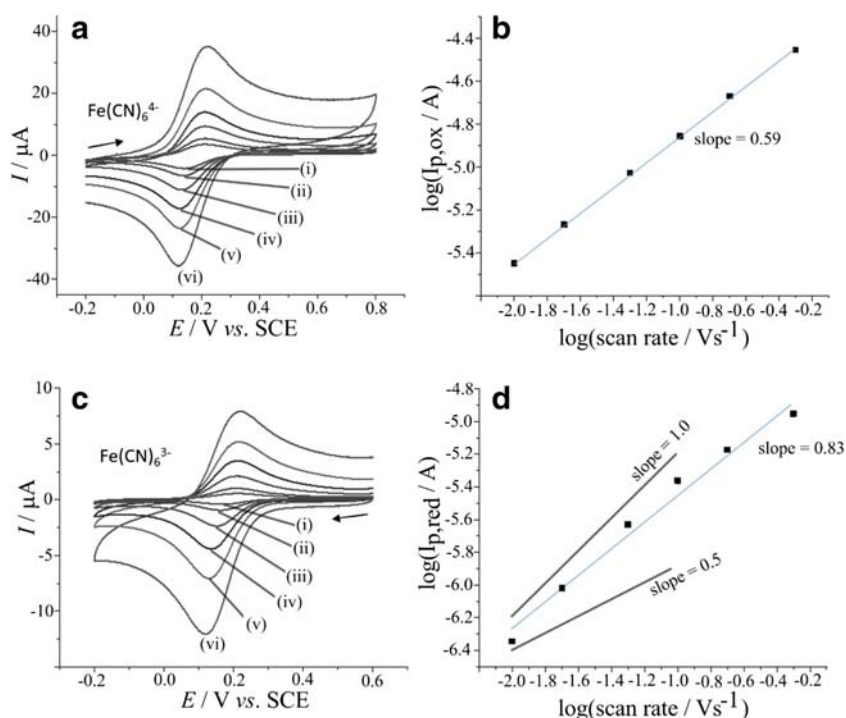
Fe(CN)$_6^{4-}$, well-defined voltammetric peaks with a peak-to-peak separation of typically 70 mV are observed. A double-logarithmic plot of anodic peak currents versus scan rate produces a slope of close to 0.5, which confirms diffusion of charges (probably via electron hopping, similar to processes reported for immobilised proteins [53]) within the micropo-rous host structure. At the slowest scan rate, 10 mV s^{-1}, the charge under the reduction peak corresponds to approx. 0.6 nmol, which is equivalent to 10% of the monomer units (estimated from the weight of polymer deposit). Given that several monomer units may be required for binding each multi-valent anion, a substantial part of the film deposit must be active under these conditions. This result also suggests that a substantial fraction of the binding sites in the PIM-EA-TB film is occupied by Fe(CN)$_6^{3-/4-}$ complexes.

The oxidation of Fe(II) to Fe(III) has to be accompanied by either a proton expulsion or a K$^+$ expulsion from the polymer host film to maintain bulk charge neutrality. When immobilising Fe(CN)$_6^{3-}$, a similar argument would suggest that the reduction of Fe(III) to Fe(II) is accompanied by cation uptake from the electrolyte. Data in Fig. 5c demonstrate a smaller peak-to-peak separation and lower peak current, sug-gesting a different type of behaviour for immobilised Fe(CN)$_6^{3-}$. The double-logarithmic plot of peak current ver-sus scan rate shows a slope much closer to 1.0 (only at slow scan rates) and therefore suggests thin layer reactivity of redox-active material. It seems possible that Fe(CN)$_6^{3-}$ (with a pK$_A$ < 1) is less effectively bound into the PIM-EA-TB film,

and therefore results in a different type of electrochemical activity. However, it may also be possible that the release of protons upon oxidation of Fe(CN)$_6^{4-}$ allows faster proton ex-pulsion whereas the reduction of Fe(CN)$_6^{3-}$ may be associated with slower K$^+$ uptake (see Eqs. 2 and 3).

$$Fe(CN)_6^{4-}(PIM) + H^+(PIM) \, Fe(CN)_6^{3-}(PIM)$$
$$+ H^+(aq) + e^- \tag{2}$$

$$Fe(CN)_6^{3-}(PIM) + K^+(aq) + e^- \, Fe(CN)_6^{4-}(PIM)$$
$$+ K^+(PIM) \tag{3}$$

Next, the effect of polymer loading is investigated. Figure 6 a shows data obtained after immobilisation in 1 mM Fe(CN)$_6^{4-}$ and transfer into 0.1 M KCl with 1 mM HCl. Stable voltammetric responses are obtained with an increase in cur-rent from 2 to 4 to 6 μg PIM-EA-TB deposit. Additional polymer then decreases the current peaks. The observed de-crease is likely to be the result of a slower uptake (the diffusion time for Fe(CN)$_6^{4-}$ in PIM-EA-TB immersed in 1 mM HCl at 4 °C is likely to be very slow). However, the current under-standing of thickness effects is very limited and more work will be required to reveal ion mobilities in these rigid host structures. A deposit of 2 μg appears appropriate and is there-fore used in all the other experiments reported here.

The effect of HCl concentration in the deposition solution on Fe(CN)$_6^{4-}$ immobilisation is demonstrated in Fig. 6b. A
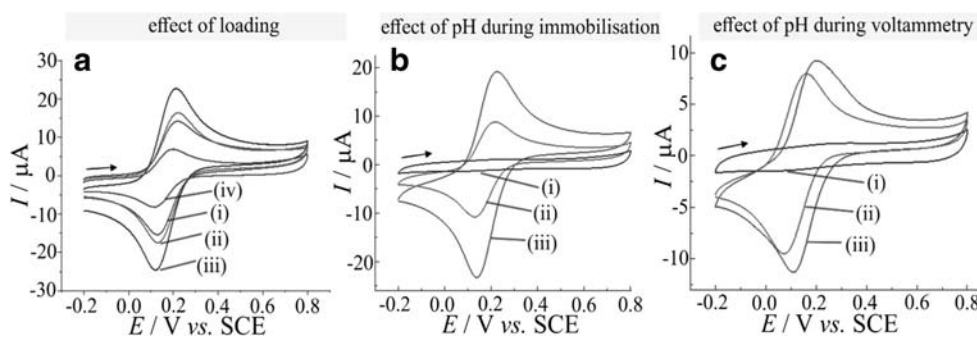
Fig. 6 a Cyclic voltammograms (first cycle; scan rate 200 mVs^{-1}; immersed in 0.1 M KCl with 1 mM HCl) for a 3-mm diameter glassy carbon electrode coated with (i) 2, (ii) 4, (iii) 6, and (iv) 8 μg PIM-EA-TB after immersion for 12 h in 1 mM Fe(CN)$_6^{4-}$/1 mM HCl. **b** Cyclic voltammograms (scan rate 100 mVs^{-1}; immersed in 0.1 M KCl with 1 mM HCl) for a glassy carbon electrode coated with 2 μg PIM-EA-TB after immersion for 12 h at 4 °C in 1 mM Fe(CN)$_6^{4-}$ in (i) 0.1, (ii) 1, and (iii) 10 mM HCl. **c** As in B but immersed in 0.1 M KCl without HCl

higher concentration of 10 mM HCl clearly enhances the resulting voltammetric peak currents with 0.1 mM HCl in the immobilisation step clearly being too low. In pH-dependent conductivity data [46], a gradual increase in degree of PIM-EA-TB protonation from pH 4 towards lower pH values was observed. This is consistent with the results observed here, and it implies a gradual change in the degree of protonation (leading to swelling and more effective immobilisation of Fe(CN)$_6^{4-}$ at increased HCl concentrations). This change in protonation appears to be retained upon taking the electrode from the 10 mM HCl solution into a pH 3 solution for cyclic voltammetry (see Fig. 6b). However, the observed peak current during cyclic voltammetry does not necessarily reflect the total amount of Fe(CN)$_6^{4-}$ binding during immobilisation due to some re-equilibration upon immersion of the electrode into the pH 3 solution. This can be shown by changing the pH of the aqueous solution during cyclic voltammetry experiments.

pH effects on the binding and reactivity of Fe(CN)$_6^{3-/4-}$ in PIM-EA-TB

In addition to the effects of pH during immobilisation of Fe(CN)$_6^{4-}$, it is interesting to explore effects of pH in the solution when performing voltammetric experiments. One would expect that for a solution pH of higher than 4, the protonation of the PIM-EA-TB should be reversed and the immobilised Fe(CN)$_6^{4-}$ should be leaching out from the PIM-EA-TB film. However, this does not happen. Experimental data in Fig. 6c show cyclic voltammetry responses observed in 0.1 M KCl (pH approx. 7). Stable voltammetric responses (over at least 10 potential cycles) are obtained consistent with those observed in pH 3 electrolyte solution. Only for the case of Fe(CN)$_6^{4-}$ immobilised in 10 mM HCl, there seems to have been some leaching out of Fe(CN)$_6^{4-}$ (see Fig. 6c (iii)). Voltammetric responses for Fe(CN)$_6^{4-}$ immobilised in the presence of 1 mM HCl are stable. This suggests that Fe(CN)$_6^{4-}$ remains immobilised in

PIM-EA-TB even in neutral solution. There are two plausible options to explain this immobilisation effect: (A) the Fe(CN)$_6^{4-}$ metal complex could form second shell interactions with K$^+$ to become more bulky and this could lead to steric retention; or perhaps more likely; (B) protonation of PIM-EA-TB is retained even at higher pH due to the requirement for hydroxide anions to enter the microporous host to annihilate the immobile protons [35]. The apparent Fe(CN)$_6^{4-}$ binding is therefore likely to be associated with the absence of hydroxide (leading to an apparently higher pK$_A$ value). The effect can be investigated by systematically changing the solution pH during cyclic voltammetry experiments.

When absorbing Fe(CN)$_6^{3-/4-}$ into the PIM-EA-TB film coating at a glassy carbon electrode surface, significant effects of pH are observed (see Fig. 6) and only protonation at a pH < 3 ensures uptake of the anions into the microporous host. In a similar way, the redox cycling of Fe(CN)$_6^{3-/4-}$ immobilised into PIM-EA-TB and immersed into aqueous electrolyte solution should be affected by pH. In particular, the effect of more alkaline pH media on the retention of the immobilised Fe(CN)$_6^{3-/4-}$ is of practical importance, as forced deprotonation with hydroxide may release Fe(CN)$_6^{4-}$ from the polymer into the solution. When loading the PIM-EA-TB film with Fe(CN)$_6^{3-}$ (from 0.1 mM Fe(CN)$_6^{3-}$ in 1 mM HCl at 4 °C in the dark) and transferring the electrode into 0.1 M KCl solution, the voltammetric response is dependent on the solution pH. Figure 7 a shows an overlay of data obtained at different pH values (pH adjusted with HCl or KOH). At pH 3, the voltammetric response shows peak currents of typically 5 to 6 μA and a midpoint potential of $E_{mid} = \frac{1}{2} (E_{p,ox} + E_{p,red}) = 0.18$ V vs. SCE. A slight loss of the voltammetric current signal occurs when going to pH 5, 7, or 9. The midpoint potential also shifts to $E_{mid} = 0.09$ V vs. SCE and remains pH independent. The shift in the midpoint potential (observed for going from pH 3 to pH 5) can be explained by proton expulsion during oxidation (see Eq. 2). The midpoint potential for the redox process then remains relatively constant from pH 5 to
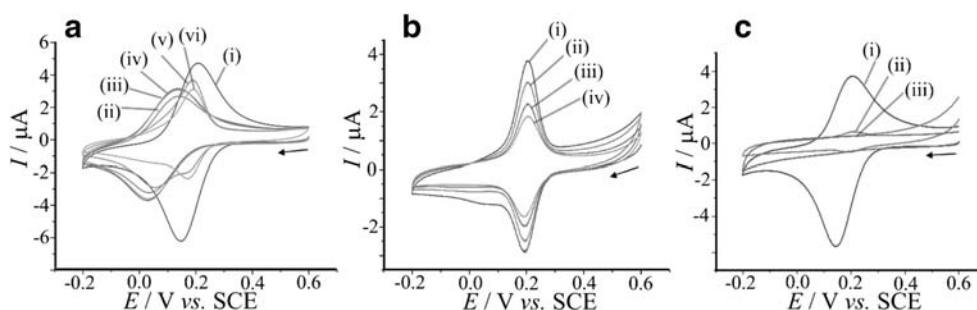
Fig. 7 **a** Cyclic voltammograms (first cycle; scan rate 0.1 Vs^{-1}) for 2 μg PIM-EA-TB (a solution of 1 mg/mL in chloroform) on a glassy carbon electrode (immersed 12 h at 4 °C into 0.1 mM K$_3$Fe(CN)$_6$ and 1 mM HCl) in aqueous 0.1 M KCl (adjusted with HCl or KOH to approx. pH (i) 3, (ii) 5, (iii) 7, (iv) 9, (v) 11 cycle 1, (vi) 11 cycle 2). **b** As before, but for pH 13 (i) cycle 1, (ii) cycle 2, (iii) cycle 5, (iv) cycle 10. **c** As before, showing (i) an initial experiment at pH 3, followed by (ii) an experiment at pH 13, then followed by (iii) an experiment at pH 3

pH 9 consistent with a process dependent on K$^+$ cations (see Eq. 3).

When changing the solution pH to more alkaline conditions (Fig. 7a), the peak response with $E_{mid} = 0.09$ V vs. SCE diminishes and a minor much more symmetric peak response with $E_{mid} = 0.20$ V vs. SCE is observed. Figure 7 b shows this new current response decaying over several potential cycles. These data can be interpreted based on the hypothesis that only at pH > 9 deprotonation of the PIM-EA-TB/H$^+$/Fe(CN)$_6^{4-}$ complex occurs, and the resulting potassium complex of Fe(CN)$_6^{4-}$ then very slowly diffuses out into the solution phase. That is, the apparent pK_A for deprotonation of PIM-EA-TB /H$^+$/Fe(CN)$_6^{4-}$ is at approx. pH 9. More fundamentally, there needs to be a significant concentration of hydroxide to cause deprotonation and leaching out of Fe(CN)$_6^{3-/4-}$. Data in Fig. 7c demonstrate that indeed after cyclic voltammetry at pH 13, the voltammetric signal for Fe(CN)$_6^{3-/4-}$ at pH 3 is also lost.

Electrocatalysis with PIM-EA-TB/Fe(CN)$_6^{3-/4-}$-coated electrodes

With Fe(CN)$_6^{3-/4-}$ immobilised in the PIM-EA-TB electrode coating, it is possible to explore catalytic behaviour. Ferrocyanide (and related cyanometalates) has been employed as a homogeneous catalyst, for example, for the detection of ascorbic acid [54] or hydrogen sulphide [6]. Furthermore, ferrocyanide immobilised into Prussian blue derivatives has been used widely for many types of redox catalytic processes. Here, the "polymeric Prussian blue" based on PIM-EA-TB/Fe(CN)$_6^{4-}$ is investigated for ascorbic acid oxidation, which is known to occur in a two-electron oxidation followed by a rapid hydration reaction step [55–57] (see Eq. 4).

Figure 8 shows voltammetric data for the electrocatalytic oxidation of ascorbic acid in aqueous 0.1 M KCl with Fe(CN)$_6^{3-/4-}$ immobilised in PIM-EA-TB. The data in Fig. 8a versus those in Fig. 8c demonstrate the effect of the

immobilisation conditions. When using 1 mM Fe(CN)$_6^{4-}$ in 1 mM HCl (Fig. 8a), the amount of Fe(CN)$_6^{4-}$ in the resulting catalyst film is lower when compared to using 0.1 mM Fe(CN)$_6^{4-}$ in 1 mM HCl (Fig. 8c). Catalytic currents are significantly higher in Fig. 8c consistent with more catalyst and/or faster charge diffusion.

Next, the effect of the solution pH during catalysis is investigated. Data in Fig. 8e have been obtained with the same type of catalytic film electrode compared to that employed in Fig. 8c, but the ascorbic acid is dissolved in 0.1 M KCl without 1 mM HCl. The oxidation of ascorbic acid does generate localise acid (see Eq. 4) but the absence of additional protons from the electrolyte appears to enhance the rate of redox catalysis.

The extent of ascorbic acid reaction can be estimated based on the Randles-Sevcik equation (see Eq. 5 [58]). In this equation, the peak current for oxidation, I_{peak}, is given by the number of transferred electrons, $n = 2$; the Faraday constant, F; the electrode area, A; the ascorbic acid concentration, c; the potential scan rate, v; the gas constant, R; the absolute temperature, T and the diffusion coefficient, D. The diffusion coefficient for ascorbic acid in water has been reported to be $D = 0.69 \times 10^{-9}$ m^{2}s^{-1} [59].

$$I_{peak} = 0.446 \, n^{3/2} F^{3/2} Ac \sqrt{\frac{vD}{RT}} \qquad (5)$$

This equation can only provide an approximate value for the current as mechanistic complications such as chemical irreversibility affect the peak current. However, an approximate line can be predicted and is shown in Fig. 8f giving the anticipated current for the diffusion-controlled oxidation of ascorbic acid, which is significantly higher compared to the observed catalytic current signals. Most likely, the observed process is limited by a combination of charge hopping and catalytic rate in the PIM-EA-TB–Fe(CN)$_6^{3-/4-}$ film deposit. More work will be required to explore porosity effects on the catalytic reaction and any significant ingress of substrate into the polymer.

Fig. 8 **a** Cyclic voltammograms (first cycle; scan rate 5 mVs^{-1}) for a 3-mm diameter glassy carbon electrode with 2 μg PIM-EA-TB (immersed into 1 mM $K_4Fe(CN)_6$ and 1 mM HCl aqueous solution at 4 °C for 12 h) in 0.1 M KCl with 1 mM HCl in the presence of (i) 0.0, (ii) 0.5, (iii) 1.0, and (iv) 2.0 mM ascorbic acid. **b** Plot of anodic peak current versus ascorbic acid concentration. **c** As above, but kept in 0.1 mM $K_4Fe(CN)_6$ in 1 mM HCl at 4 °C for 12 h and measured in 0.1 M KCl with 1 mM HCl in the presence of (i) 0.0, (ii) 0.5, (iii) 1, (iv) 4, (v) 8, and (vi) 16 mM ascorbic acid. **d** Plot of anodic peak current versus ascorbic acid concentration. **e** As above, but kept in 0.1 mM $K_4Fe(CN)_6$ in 1 mM HCl at 4 °C for 12 h and measured in 0.1 M KCl without 1 mM HCl in the presence of (i) 0, (ii) 1, (iii) 2, (iv) 4, (v) 8, and (vi) 16 mM ascorbic acid. **f** Plot of anodic peak current versus ascorbic acid concentration
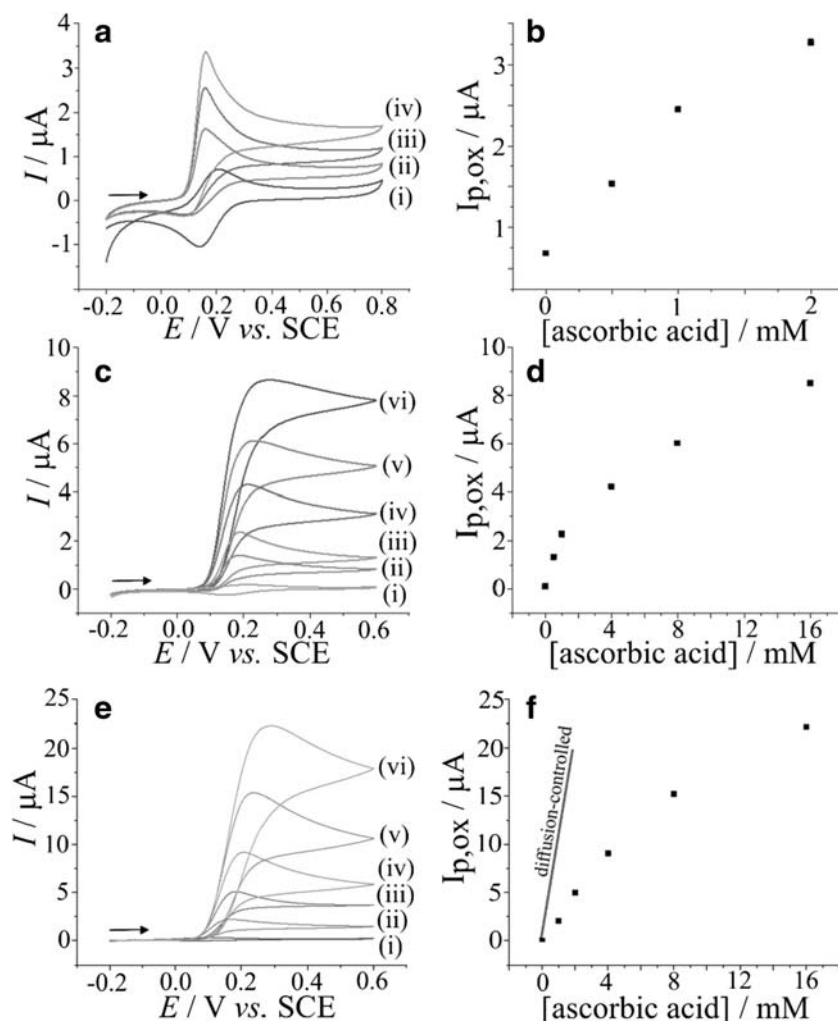
Summary and conclusions

Preliminary data reported here demonstrate the permeation and immobilisation of $Fe(CN)_6^{3-/4-}$ in a microporous PIM-EA-TB host film. Protonation of PIM-EA-TB is associated with immobilisation of $Fe(CN)_6^{3-/4-}$ and with formation of a redox-active film deposit. The 1–2-nm nanochannels in PIM-EA-TB provide space for ion transport and inter-diffusion of substrates for electrocatalytic oxidation. The main observations can be summarised as:

1. Protonation of the PIM-EA-TB material at pH 3 (at 4 °C over 12 h) results in an efficient immobilisation of $Fe(CN)_6^{4-}$. A higher concentration of acid will increase the amount of $Fe(CN)_6^{4-}$, but this increase only leads to additional leaching after transfer into ambient electrolyte media.
2. More generally, when considering permeation of anions such as $Fe(CN)_6^{4-}$ through microporous materials such as PIM-EA-TB, simple permeation rate constants (used for example for gas permeation) are flawed as counter ion effects (here for both K^+ and H^+) are clearly important.
3. $Fe(CN)_6^{4-}$ behaves as a base and is therefore competing for protons during the immobilisation process. Therefore, a high concentration of $Fe(CN)_6^{4-}$ can be detrimental to immobilisation.
4. Once immobilised in PIM-EA-TB, the $Fe(CN)_6^{4-}$ is redox-active and readily and reversibly switched to $Fe(CN)_6^{3-}$ at the electrode surface. The voltammetric response shows characteristics typical of that of diffusion processes, which is likely to be dominated by electron hopping diffusion rather than metal complex diffusion within the polymer host.
5. Electrocatalysis is observed for $Fe(CN)_6^{3-}$-mediated ascorbate oxidation with the amount of $Fe(CN)_6^{4-}$ immobilisation in PIM-EA-TB strongly affecting the apparent rate constant. This could be associated with either the rate of charge transport through the film or the ability of ascorbic acid to diffuse into the micropores.

The data presented in this preliminary study have to be seen as a first step in exploring more complex cases of ion permeation with counter ion effects coupled to redox reactivity. Data comparing the reactivity of $Fe(CN)_6^{4-}$ and $Fe(CN)_6^{3-}$ under similar conditions is incomplete and even models for the comparison of these two types of immobilised anions during voltammetry are incomplete. Much more work will be required on kinetic aspects and on application of these (and similar) systems.

In the future, modification of the molecular structure of PIM-EA-TB could be used to further tune the properties, stability and reactivity of these hybrid films. In addition to $Fe(CN)_6^{3-/4-}$ a wider range of poly-anions are likely to be possible guest species for redox catalysis. Prussian blue analogous coordination polymer systems could also be embedded into microporous hybrid films for applications in electrocatalysis.

References

1. Nematollahi D, Varmaghani F (2008) Electrochim Acta 53:3350–3355
2. Thorne RJ, Hu HN, Schneider K, Cameron PJ (2014) Phys Chem Chem Phys 16:5810–5816
3. Buckingham MA, Marken F, Aldous L (2018) Sustain. Energy Fuel 2:2717–2726
4. Zhang H, Li J, Wang K, Du XZ, Li QM (2009) Anal Biochem 388:40–46
5. Almeida PL, Mendes CHS, Lima IAFS, Belian MF, Oliveira SCB, Brett CMA, Nascimento VB (2018) Anal Lett 51:496–511
6. Jeroschewski P, Steuckart C, Kuhl M (1996) Anal Chem 68:4351–4357
7. Lawrence NS, Thompson M, Prado C, Jiang L, Jones TGJ, Compton RG (2002) Electroanalysis 14:499–504
8. Niu WJ, Zhu RH, Cosnier S, Zhang XJ, Shan D (2015) Anal Chem 87:11150–11,156
9. Chang JL, Wei GT, Chen TY, Zen JM (2013) Electroanalysis 25:845–849
10. Jones TR, Hernandez-Aldave S, Kaspar RB, Letterio MP, Yan YS, Bertoncello P (2019) Electrochim Acta 311:160–169
11. Itaya K, Uchida I, Neff VD (1986) Acc Chem Res 19:162–168
12. Azhar A, Li YC, Cai ZX, Zakaria MB, Masud MK, Hossain MSA, Kim J, Zhang W, Na J, Yamauchi Y, Hu M (2019) Bull Chem Soc Japan 92:875–904
13. Alexandrov EV, Virovets AV, Blatov VA, Peresypkina EV (2015) Chem Rev 115:12286–12,319
14. Karyakin AA (2001) Electroanalysis 13:813–819
15. Koncki R (2002) Crit Rev Anal Chem 32:79–96
16. Chu Z, Liu Y, Jin WQ (2017) Biosens Bioelectron 96:17–25
17. de Mattos IL, Gorton L (2001) Quim Nova 24:200–205
18. Schröder U, Scholz F (2000) Inorg Chem 39:1006–1015
19. Dussel H, Dostal A, Scholz F (1996) Fresenius J Anal Chem 355:21–28
20. Dostal A, Meyer B, Scholz F, Schröder U, Bond AM, Marken F, Shaw SJ (1995) J Phys Chem 99:2096–2103
21. Cvrtila I, Stilinović V (2017) Cryst Growth Design 17:6793–6800
22. Pejaković DA, Manson JL, Miller JS, Epstein AJ (2001) Synth Met 122:529–533
23. Ksenofontov V, Levchenko G, Reiman S, Gütlich P, Bleuzen A, Escax V, Verdaguer M (2003) Phys Rev B 68:024415
24. Epstein AJ (2000) MRS Bull 25:33–40
25. McKeown NB, Budd PM (2006) Chem Soc Rev 35:675–683
26. McKeown NB, Budd PM (2010) Macromolecules 43:5163–5176
27. Dawson R, Cooper AI, Adams DJ (2012) Prog Polym Sci 37:530–563
28. Chaoui N, Trunk M, Dawson R, Schmidt J, Thomas A (2017) Chem Soc Rev 46:3302–3321
29. Low ZX, Budd PM, McKeown NB, Patterson DA (2018) Chem Rev 118:5871–5911
30. Rong YY, Song QL, Mathwig K, Madrid E, He DP, Niemann RG, Cameron PJ, Dale SEC, Bending S, Carta M, Malpass-Evans R, McKeown NB, Marken F (2016) Electrochem Commun 69:41–45
31. Madrid E, McKeown NB (2018) Curr Opinion Electrochem 10:61–66
32. Marken F, Madrid E, Zhao YZ, Carta M, McKeown NB (2019) ChemElectroChem 6:4332–4342
33. Carta M, Malpass-Evans R, Croad M, Rogan Y, Jansen JC, Bernardo P, Bazzarelli F, McKeown NB (2013) Science 339:303–307
34. Yushkin A, Vasilevsky V, Khotimskiy V, Szymczyk A, Volkov A (2018) J Membr Sci 554:346–356
35. Kolodziej A, Ahn SD, Carta M, Malpass-Evans R, McKeown NB, Chapman RSL, Bull SD, Marken F (2015) Electrochim Acta 160:195–201
36. Rong YY, Kolodziej A, Madrid E, Carta M, Malpass-Evans R, McKeown NB, Marken F (2016) J Electroanal Chem 779:241–249
37. Zhuang XM, Wang DL, Lin YQ, Yang LF, Yu P, Jiang W, Mao LQ (2012) Anal Chem 84:1900–1906
38. Gomez-Romero P, Ayyad O, Suarez-Guevara J, Munoz-Rojas D (2010) J Solid State Electrochem 14:1939–1945
39. Zhao W, Xu JJ, Shi CG, Chen HY (2005) Langmuir 21:9630–9634
40. Chaudhary A, Pathak DK, Tanwar M, Sagdeo PR, Kumar R (2019) ACS Appl Electronic Mater 1:892–899
41. Tieke B (2011) Curr Opinion Coll Interface Sci 16:499–507
42. DeLongchamp DM, Hammond PT (2004) Adv Funct Mater 14:224–232
43. Lapidus SH, Graham AG, Kareis CM, Hawkins CG, Stephens PW, Miller JS (2019) J Amer Chem Soc 141:911–921
44. Nai JW, Lou XW (2019) Adv Mater 31:1706825
45. Namgung H, Gwon YJ, Kim J, Jang G, Pepper SE, Ogden MD, Whittle KR, Harwood LM, Lee TS (2018) Polymer 158:320–326
46. Madrid E, Rong YY, Carta M, McKeown NB, Malpass-Evans R, Attard GA, Clarke TJ, Taylor SH, Long YT, Marken F (2014) Angew Chem Int Ed 53:10751–10,754
47. Marcus Y (1997) Ion Properties, Marcel Dekker, New York, 54
48. Rong YY, He DP, Sanchez-Fernandez A, Evans C, Edler KJ, Malpass-Evans R, Carta M, McKeown NB, Clarke TJ, Taylor

SH, Wain AJ, Mitchels JM, Marken F (2015) Langmuir 31:12300–12,306

49. Jordan J, Ewing GJ (1962) Inorg Chem 1:587–591

50. Sutter JR, Spencer W (1990) J Phys Chem 94:4116–4119

51. Koncki R, Wolfbeis OS (1998) Anal Chem 70:2544–2550

52. Tan R, Wang AQ, Malpass-Evans R, Williams R, Zhao EW, Liu T, Ye CC, Zhou XQ, Primera Darwich B, Fan ZY, Turcani L, Jackson E, Chen LJ, Chong SY, Li T, Jelfs KE, Cooper AI, Brandon NP, Grey CP, McKeown NB, Song QL (2020) Nat Mater 19:195–202

53. McKenzie KJ, Marken F (2003) Langmuir 19:4327–4331

54. Thangamuthu R, Wu Y-C, Chen S-M (2009) Electroanalysis 21:165–171

55. Perone SP, Kretlow WJ (1966) Anal Chem 38:1763–1767

56. Lechien A, Valenta P, Ntirnberg HW, Patriarche GJ (1982) Fresenius Z Anal Chem 3:105–108

57. Hian LC, Grehan KJ, Compton RG, Foord JS, Marken F (2003) Diam Relat Mater 12:590–595

58. Scholz F (2010) Electroanalytical Methods 2nd, Springer, Berlin, 70

59. Motshakeri M, Travas-Sejdic J, Phillips ARJ, Kilmartin PA (2018) Electrochim Acta 265:184–193